

# UNIDIRECTIONALLY COUPLED MAP LATTICES WITH NON-LINEAR COUPLING: UNBINDING TRANSITIONS AND SUPER-LONG TRANSIENTS

CHRISTIAN MARSCHLER\* AND JÜRGEN VOLLMER†

**Abstract.** Recently, highly resolved experiments and simulations have provided detailed insight into the dynamics of turbulent pipe flow. This has revived the interest to identify mechanisms that generate chaotic transients with super-exponential growth of lifetime as a function of a control parameter, the Reynolds number for pipe flow, and with transitions from bounded chaotic patches to an invasion of space of irregular motion. Dynamical systems models are unique tools in this respect because they can provide insight into the origin of the very long life time of puffs, and the dynamical mechanism leading to the transition from puffs to slugs in pipe flow. The present paper contributes to this enterprise by introducing a unidirectionally coupled map lattice. It mimics three of the salient features of pipe-flow turbulence: (i) the transition from laminar flow to puffs, (ii) a super-exponential scaling of puff lifetime, and (iii) the transition from puffs to slugs by an unbinding transition in an intermittency scenario. In our model all transitions and scalings are theoretically described from a dynamical systems point of view.

**Key words.** coupled map lattice, unidirectional coupling, nonlinear coupling, intermittency, unbinding transition, pipe flow, turbulence lifetime, spreading of turbulence

**AMS subject classifications.** 37N10, 76F06, 76F20

**1. Introduction.** More than 100 years ago Reynolds [37] established that the qualitative behavior of pipe flow is described by a single control parameter, the Reynolds number  $Re$ , while details of trajectories depend on the specific initial conditions. For all  $Re$  a parabolic flow profile appears to be stable [28, 43]. However, for  $1750 \lesssim Re \lesssim 2200$  there emerges another solution [27]: long-living chaotic transients of a fixed finite-size, *turbulent puffs*, that are advected down the pipe with the mean flow. Their dynamics shows sensitive dependence on initial conditions [13], and for any given Reynolds number the lifetime of individual puffs is exponentially distributed [13, 22, 33, 20]. There appears to be no critical Reynolds number where the lifetime of the puffs diverges. Rather, recent experimental data suggest [20] that the mean lifetime  $\tau$  grows super-exponentially like  $\log \log \tau \sim Re$ , in accordance with direct numerical simulations [6]. For  $Re \gtrsim 2200$  there is an increasing probability for puff splitting [43, 29, 4]. A critical point for this transition has been shown to emerge at  $Re = 2040$  [4], marking the cross-over between two processes: decay of turbulence by the decay of puffs, and its spreading by puff splitting. Eventually the splitting leads to a constant growth of the turbulent regions in the pipe, *turbulent slugs*. Numerical simulations for pipe flow reveal highly non-linear, i. e., non-diffusive, coupling in the downstream direction [12, Fig. 18], where intermittently very strong azimuthal vorticity perturbations are generated close to the pipe wall. Subsequently, they propagate to the center of the pipe where they are accelerated and enhance turbulence downstream the pipe.

The important role played by the nonlinear forward coupling in pipe flow motivates us to study the consequences of non-linear forward coupling from a dynamical

---

\*Technical University of Denmark, Department of Applied Mathematics and Computer Science, Matematiktorvet 303B, DK-2800 Kgs. Lyngby, Denmark, and Max Planck Institute for Dynamics and Self-Organization, Fassberg 17, D-37077 Göttingen, Germany (c.marschler@mat.dtu.dk).

†Max Planck Institute for Dynamics and Self-Organization, Fassberg 17, D-37077 Göttingen, Germany, and Institute for Nonlinear Dynamics, Faculty of Physics, Georg August University, D-37077 Göttingen, Germany (juergen.vollmer@ds.mpg.de).

systems perspective. We establish a coupled map lattice (CML) where puffs are instances of super-long transients in dynamical systems [41]. CMLs are dynamical systems where the dynamic quantities take continuous values defined on a discrete set of lattice sites, and where these values are updated at discrete times according to a deterministic rule. Our CML features a transiently chaotic on-site dynamics and a non-linear, unidirectional coupling between lattice sites.

CMLs have been studied extensively for diffusively-coupled, chaotic on-site dynamics [8, 9]. In particular, the study of spatio-temporal intermittency, chaos and supertransients [23, 24, 25, 10, 17, 42] and the control of chaos [14, 32, 31] gained much attention. Applications reach from front motion in hydrodynamic models [34], to modelling of traffic flow [44] and evolution of genetic sequences [11]. In Refs. [38, 39] advectively-diffusively coupled map lattices have been studied as a model for open flow, addressing in particular the relation to turbulent pipe flow and to spatio-temporal intermittency [36, 23, 10, 35]. A recent model along this line picked up this approach to gain insight into the transition from puffs to slugs in turbulent pipe flow [7].

Unidirectionally coupled map lattices (UCML) were introduced in Ref. [38] in order to address the transition to turbulence in open flows. UCMLs provide a minimalistic approach to understand the dynamics and transitions, i. e., bifurcations in the dynamics of turbulent pipe flow. However, in contrast to the models considered previously [38, 7] our UCML has a non-linear coupling. As a consequence the model is complicated enough to show the complex behavior observed in turbulent pipe flow. On the other hand, it is simple enough so that we can analytically discuss the bifurcation points for the transitions from laminar flow to turbulent puffs (Section 4.2) and from puffs to slugs (Section 4.1).

The paper is structured as follows. In Section 2 we introduce our model. Section 3 gives numerically computed sample trajectories for different parameter values to get an idea about the different solutions of the system. Section 4 explains the main results and compares analytical and numerical findings. In particular, the transitions from laminar pipe flow to puffs, and from puffs to slugs are presented in Sections 4.2 and 4.1, respectively. A lifetime analysis of puffs is presented in Section 4.3, and the implications of our model to the qualitative understanding of pipe-flow turbulence is further discussed in Section 5. The paper concludes with a summary and an outlook to future research directions in Section 6.

**2. Model.** In this section, we define our unidirectionally coupled map lattice (UCML). It is defined on a one-dimensional lattice with sites  $i \in \{1, \dots, m\}$ .

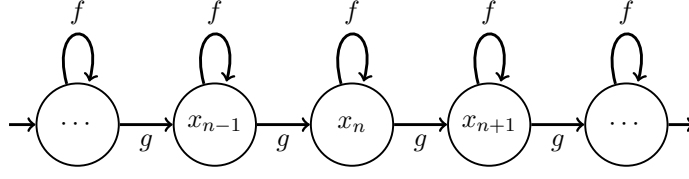
We represent the state of the system at site  $i$  and time  $t \in \mathbb{N}$  by variables  $x_t^i \in \mathbb{R}$  which mimic the turbulent kinetic energy of the flow. For a laminar flow, i. e., the stable stationary solution for the pipe flow problem, this variable takes values  $x_t^i = 0$ .

The evolution of the state variables  $x_t^i$  follows a coupled map lattice dynamics

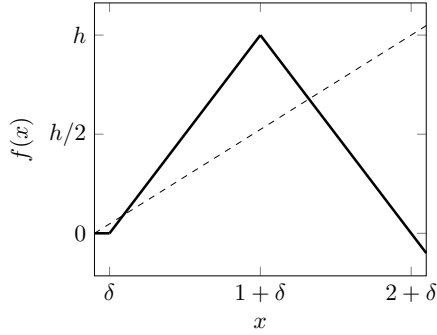
$$x_{t+1}^i = \alpha g(x_t^{i-1}) + f(x_t^i), \quad (2.1)$$

where  $f$  generates an on-site dynamics, and  $\alpha g$  is a *unidirectional* coupling of sites  $i$  and  $i - 1$  with coupling strength  $\alpha$  (cf. Fig. 2.1).

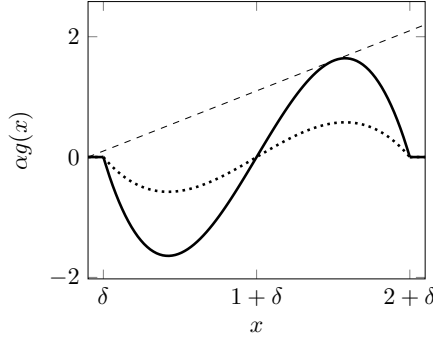
The substantial difference to previous approaches [7, 10, 17, 25, 38, 15] lies in our choice of the coupling. In contrast to other coupled map lattice models, which address diffusive and advective coupling (see e. g., [10, 24, 25, 38, 7]), we adopt a non-linear



(a) Sketch of the unidirectionally coupled map lattice.



(b) On-site dynamics  $f$ .



(c) Coupling function  $\alpha g$ .

FIG. 2.1. (a) Sketch of our unidirectionally coupled map lattice. The on-site dynamics is given by the function  $f$ , and the coupling function  $g$  determines the forward coupling, mimicking the downstream of pipe flow. (b) The on-site dynamics  $f$  is a shifted tent map Eq. (2.3), which is cut off at  $\delta$ . Intersections with the diagonal (dashed line) denote fixed points. For  $h > 2$ , almost all trajectories are transients to the globally stable fixed point at  $x = 0$ . (c) The coupling function  $\alpha g$  for the forward coupling takes the form specified in Eq. (2.2). For  $\alpha < \alpha_{sn}$  (dotted curve), it has a single fixed point  $x = 0$ . At  $\alpha = \alpha_{sn}$  (solid curve), another pair of fixed points is born in a saddle-node bifurcation.

unidirectional coupling (cf. Fig. 2.1(c))

$$g(x) = \begin{cases} -\frac{3}{2} (x - \delta) (x - 1 - \delta) (x - 2 - \delta), & \delta \leq x < 2 + \delta \\ 0, & \text{else.} \end{cases} \quad (2.2)$$

In our choice to provide only a forward coupling we follow Ref. [38, 39]. The choice of a nonlinear coupling function is motivated by the numerical results shown in Fig. 18 of [12], where spatial intermittency in pipe flow is connected to the fast forward propagation of vorticity perturbations generated at the edge of the pipe. This finding points to a strong, nonlinear downstream coupling in pipe flow. It motivates us to choose a non-linear coupling along the lattice that provides an intermittent dynamics close to the saddle-node bifurcation of  $\alpha g$  (cf. Fig. 2.1(c) and Eq. (4.2) below). Hence, the action of the function  $g$  models the propagation of turbulence in puffs and slugs. The specific choice of  $g$  is generic as long as the maximum in the right domain  $x \in [1 + \delta, 2 + \delta]$  allows for an intermittency scenario via a saddle-node bifurcation.

In line with previous approaches [10, 15, 7] the on-site dynamics is generated by a modified tent map (Fig. 2.1(b)),

$$f(x) = \begin{cases} h (x - \delta), & \delta \leq x < 1 + \delta \\ -h (x - 2 - \delta), & 1 + \delta \leq x \\ 0, & \text{else.} \end{cases} \quad (2.3)$$

It is augmented with a flat piece close to the origin  $[0, \delta]$  in accordance with the requirement that  $x = 0$  is a globally stable fixed point. For  $h > 1$ , the on-site dynamics has three fixed points

$$x_0^f = 0, \quad x_1^f = \frac{h\delta}{h-1}, \quad x_2^f = \frac{h(2+\delta)}{1+h}, \quad (2.4)$$

where  $x_0^f$  is stable, and  $x_1^f, x_2^f$  are unstable. The specific form of the cutoff towards the very small values of  $x$  does not affect the scaling of the transitions to be discussed in the following, as long as  $x = 0$  remains a globally stable fixed point. For the purpose of the present study the offset is kept fixed,  $\delta = 0.1$ . Follow up studies that strive for a quantitative comparison with pipe flow will have to account for the shrinking of the basin of attraction for the laminar flow with  $\text{Re}$  (see [21]) in real pipe flow. Further studies of system (2.1) could include a dependence  $\delta(\alpha, h)$ , effectively modelling  $\delta(\text{Re})$ , and reducing the number of free parameters in our UCML. Since  $Df(x_0^f) \equiv 0$ , the state  $x_t^i = 0$  for all  $i$  is a stable fixed point of the dynamics for all parameter values. It mimics laminar flow. Furthermore, a turbulent state is identified with values  $x_t^i > 0$ . For all numerical simulations periodic boundary conditions are enforced. During simulations, the lattice is always chosen long enough to ensure, that the leading edge never meets the trailing edge, i. e., an infinitely-long pipe is modelled.

For  $h > h_c = 2$  the map  $f$  shows transient chaotic behavior with an exponential distribution of lifetime  $\tau$  whose average

$$\tau_s = \left[ \ln \frac{h}{h_c} \right]^{-1} \quad (2.5)$$

diverges algebraically as  $h$  approaches  $h_c = 2$  [18, 30].

The slope  $h$  of the tent map and the coupling strength  $\alpha$  serve as control parameters of the dynamics. In Sections 3 and 4 we analyze the behavior of this dynamical system in response to varying the control parameters  $h$  and  $\alpha$ . The connection to pipe flow is detailed in Section 4 where we discuss how the parameters can be connected to the Reynolds number,  $\text{Re}$ . For the discussion of the dynamical systems aspects of the transitions this approach is more transparent, and in order to see their physical implications it is sufficient to observe that increasing  $\text{Re}$  amount to an increasing  $\alpha$  and decreasing  $h$ . We also refrain from identifying a specific frame of reference for the velocities because it will depend in detail of the connection of the nonlinear coupling function,  $g$ , and the intermittent forward coupling in pipe flow which we do not explore with our generic choice of  $g$ .

**3. Numerical Results.** In order to provide an overview about the solutions of the UCML, we discuss trajectories for different parameter values. Changing the coupling parameter  $\alpha$  and the height of the tent map  $h$ , three qualitatively different types of solutions are observed: (i) immediately decaying structures; (ii) propagating turbulent puffs, i. e., constant size turbulent spots that are advected downstream (cf. Fig. 3.1(a) and Fig. 3.1(b)); (iii) turbulent slugs, i. e., growing turbulent regions (cf. Fig. 3.1(c)).

In Eq. (2.5) the scaling of the lifetime of the on-site dynamics is stated for values  $h > h_c = 2$ . For  $h < h_c$  chaotic on-site motion does not decay. As a consequence, the chaotic dynamics is only spreading due to the coupling and there will be no fluctuations where the systems relaminarizes at times. Such a dynamics is not of interest to model pipe flow [5]. Therefore, in the following we only investigate solutions

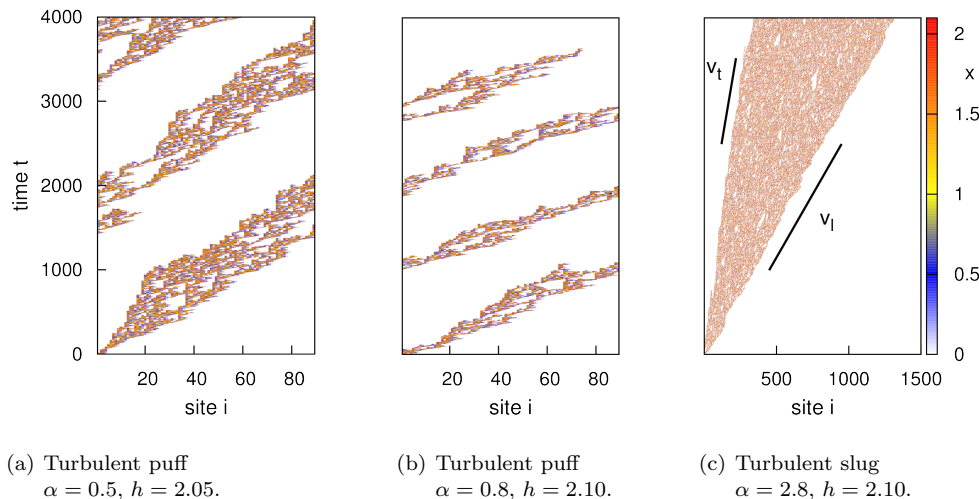


FIG. 3.1. Space-time plots of the UCML, Eq. (2.1). The color represents the values of  $x$  as specified by the color bar to the right. (a) For intermediate values of the coupling,  $\alpha = 0.5$ ,  $h = 2.05$ , there are chaotic regions of a fixed average size that propagate with a finite speed. (b) For a different set of parameters,  $\alpha = 0.8$ ,  $h = 2.10$ , the lifetime of turbulent puffs can be much shorter. (c) For higher coupling,  $\alpha = 2.8$ ,  $h = 2.10$ , the chaotic region increases linearly in size. The time axes are identical for all three plots; beware however the different system size.

for  $h > h_c$ . The numerical observations suggest, that there are two critical parameter values for the coupling strength:  $\alpha_P$  and  $\alpha_{sn}$ .

For  $\alpha \in [0, \alpha_P]$ , the coupling is not strong enough to kick the adjacent lattice site into a turbulent state. A finite single-site initial perturbation decays unless it is exactly initialized at an unstable periodic orbit of  $f$ . The probability to be found in a turbulent state for  $t$  successive time steps decays exponentially with the decay rate of the on-site dynamics,  $\tau_s^{-1}$ .

For  $\alpha \gtrsim \alpha_P$ , an initial perturbation spreads if  $2 + \delta > x > 1 + \delta$ , i.e., for  $x$  where  $g(x) > 0$ . For unidirectional couplings the transient dynamics of  $f$  also governs the decay of turbulence at the rear side of the turbulent structures. It reaches a certain width. Eventually, a constant number of sites are in a turbulent state, and this finite-size structure travels through the lattice in the direction given by the coupling (Fig. 3.1(a) and Fig. 3.1(b)). This dynamics is reminiscent of turbulent puffs and it is observed numerically in the UCML, that the lifetime depends on the parameters. In Fig. 3.1(b), a puff solution with a relatively small width and short lifetime is shown. After about 3500 time steps, the puff decays to the laminar state. For a different set of parameters, there are broader structures with a longer lifetime (Fig. 3.1(a)). Upon increasing the coupling strength  $\alpha$  or decreasing  $h$  towards  $h_c$  the average lifetime of puffs rises, and eventually, there is a transition to slug-like dynamics (Fig. 3.1(c)): the velocity at the leading edge,  $v_l$ , is higher than the velocity at the trailing edge,  $v_t$ , such that the turbulent structures broaden while traveling through the lattice. Hence, we find solutions reminiscent of turbulent slugs.

For  $\alpha > \alpha_{sn}$ , the coupling function  $\alpha g$  attains a non-trivial fixed point that induces ballistic propagation of the leading edge of the slug,  $v_l = 1$ .

In Section 4 we provide a detailed study of the transitions.

**4. Analytical Treatment.** In this section, the critical couplings  $\alpha_P$  and  $\alpha_{sn}$  are computed analytically, and their dependence on  $h$  is discussed (see Fig. 4.2). All predictions are verified by comparing to numerically obtained results. We first focus on the growth speed of the turbulent region in the slug regime, i. e., on the parameter dependence of the difference  $v_l - v_t$  of the propagation velocity  $v_l$  of the leading edge and the one  $v_t$  of the trailing edge of the turbulent region, as shown in Fig. 3.1(c). Subsequently, we address the factors governing the lifetime of puffs (cf. Fig. 3.1(a) and Fig. 3.1(b)).

**4.1. Slugs.** Since there is only forward coupling of the dynamics, the lifetime of the site at the trailing edge, i. e., the last non-zero site of the slug amounts to the lifetime,  $\tau_s(h)$ , of chaotic transients of the on-site dynamics,  $f$ . The velocity  $v_t$  should hence be a function of  $h$  only. This is confirmed by the data to the lower right in Fig. 4.1. Using Eq. (2.5), the average propagation velocity of the trailing edge is estimated as

$$v_t \simeq \frac{1}{\tau_s(h)} = \ln \frac{h}{h_c}. \quad (4.1)$$

The solid red line in Fig. 4.1 shows that Eq. (4.1) is a lower bound for the trailing edge velocity. It is a sharp bound when the single-site lifetimes are large, i. e., for  $h$  close to  $h_c$ . The mismatch for larger  $h$  is due to jumps by several sites, when the right neighbors of the trailing site are already in the laminar state. The decay of the turbulent dynamics of that site leads then to a jump of the trailing border of the slug by more than a single site, and hence to a higher propagation velocity. This effect becomes more pronounced when there is a larger number of laminar sites within the turbulent region, i. e., when  $\tau_s$  decreases due to an increase of  $h$ . It is evident from Fig. 3.1 that the time scale  $\tau_s$  is much shorter than the turbulence lifetime  $\tau$ . After all, turbulence is sustained by propagation along the system. In particular, turbulence persists when the trailing edge can not catch up with the leading edge.

The propagation velocity at the leading edge of the slug, i. e., the right-most site with non-vanishing  $x$ , is governed by  $\alpha g$ . Hence, we expect that the velocity  $v_l$  should be a function of  $\alpha$ . In order to gain insight into the propagation we start from strong coupling. For  $\alpha = \alpha_{sn} \simeq 2.844137$  there is a saddle-node bifurcation where a fixed point  $x^f$  emerges in the coupling function  $\alpha g$  (cf. Fig. 2.1(c)),

$$\alpha_{sn} g(x^f) = x^f, \quad \alpha_{sn} g'(x^f) = 1. \quad (4.2)$$

Beyond this bifurcation, i. e., for  $\alpha > \alpha_{sn}$ , the stable fixed point leads to a ballistic propagation of the front. This behavior can be understood by analyzing the case  $\alpha = \alpha_{sn}$ . If  $(x_t^i, x_{t+1}^{i+1}) = (x^f, 0)$ , then according to Eq. (2.1)  $x_{t+1}^{i+1} = x^f$ . The turbulence propagates to the next site in each time step; a front edge at  $x = x^f$  propagates ballistically.

Immediately before the bifurcation, i. e., for  $\Delta\alpha \equiv \alpha_{sn} - \alpha \ll 1$ , trajectories can spend a time  $T$  in the vicinity of  $x^f$  such that the propagation velocity can be estimated as an average of a fast propagation when  $x \simeq x^f$  and slow propagation for other values of  $x$ .

According to Little's lemma [26] propagation is observed with probability

$$p(\Delta\alpha) = [1 + 1/(\nu T)]^{-1}, \quad (4.3)$$

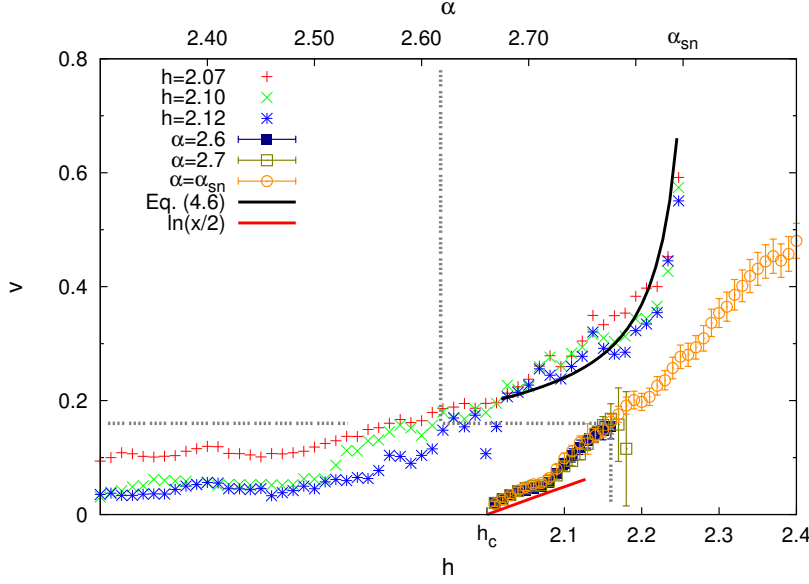


FIG. 4.1. The average propagation velocities  $v_l(\alpha)$  and  $v_t(h)$  of the leading (upper left data sets, top axis) and the trailing edge (lower right data sets, bottom axis), respectively. The solid black and red lines provide analytical estimates for  $v_l$  and  $v_t$ , respectively, and the gray, dotted line is used to construct the transition line  $\alpha_{PS}(h)$  from puffs to slugs (cf. main text for details). The displayed values for both velocities are obtained by averaging over  $2 \times 10^4$  initial conditions. Corresponding standard deviations are of the order of 0.05 for  $\alpha$  close to  $\alpha_{sn}$ , and increase to about 0.1 for  $\alpha \lesssim 2.5$ .

where  $\nu$  is the injection rate into the vicinity of the emerging fixed point. Eq. (4.3) can be understood intuitively by considering a 2-state Markov chain, where  $p$  and  $q$  are the probabilities to be in the propagating and non-propagating state, respectively. Further, we denote the transition rate from state  $p$  to  $q$  with  $\nu_{out}$  and the one from  $q$  to  $p$  with  $\nu$ . Employing the normalization  $1 = p + q$  and the steady-state assumption  $\dot{p} = \dot{q} = 0$ , we obtain Eq. (4.3), where the escape rate is  $\nu_{out} = 1/T$ . Moreover, the scaling of lifetimes in the intermittency scenario [36, 30] for the “stickiness” of the coordinate  $x^f$ , states that

$$T = a \Delta\alpha^{-\frac{1}{2}}, \quad (4.4)$$

which is the mean time to escape a narrow tunnel just before a saddle-node bifurcation (cf. the type-I intermittency scenario in [30]). In the present case the factor of proportionality amounts to  $a \simeq 1.55$  and has been fitted to simulation data.  $\Delta\alpha$  denotes the distance to the saddle-node bifurcation in  $g$ . Moreover, the entrance probability to the region can be evaluated following recent ideas on Poincaré recurrences [2, 3],

$$\nu = \nu_c + A \exp(-\Delta\alpha/\xi) \quad (4.5)$$

with  $\nu_c = 0.039$ ,  $A = 0.034$  and  $\xi = 0.023$  obtained by fits to simulation data for the present map. For  $\alpha$  values below the bifurcation,  $2.7 \lesssim \alpha < \alpha_{sn}$  and using Eq. (4.3), Eq. (4.4) and Eq. (4.5), we thus obtain an explicit expression for the spreading velocity

$$v_l \simeq p(\Delta\alpha) = \left[ 1 + \frac{\Delta\alpha^{\frac{1}{2}}}{a(\nu_c + A \exp(-\Delta\alpha/\xi))} \right]^{-1}. \quad (4.6)$$

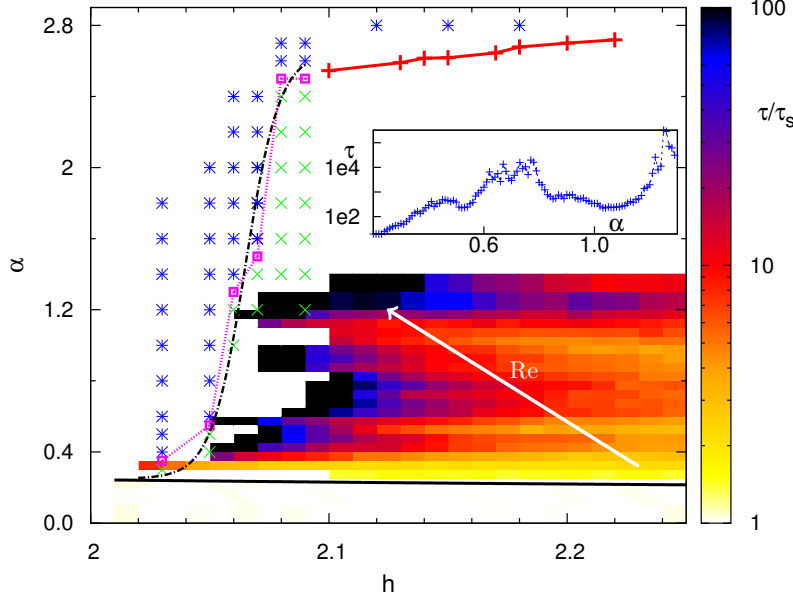


FIG. 4.2. Phase diagram for the qualitative behavior of chaotic transients of the UCML dynamics Eq. (2.1). For  $\alpha < \alpha_P \simeq 0.23$  (solid black line) chaotic behavior does not propagate along the system and transients have an average lifetime  $\tau_s$ . The lifetime of puffs is shown in false color according to the legend to the right of the plot. Green crosses mark puffs with a lifetime  $\tau > 10^3 \tau_s$  from single trajectories, and slugs are indicated by blue stars. The dotted black line marks the transition from puffs to slugs upon decreasing  $h$ , and the solid red line is the border  $\alpha_{PS}$  as determined from Fig. 4.1 (cf. main text). The white arrow indicates the trends how  $\alpha$  and  $h$  change upon increasing Reynolds number. The inset shows the lifetime  $\tau$  as a function of  $\alpha$  for fixed  $h = 2.1$ .

It is indicated by a solid black line in Fig. 4.1 and helps us to understand the leading edge velocity and thereby the transition from puffs to slugs.

The key element is the possibility of a bifurcation analysis at an unphysical parameter value  $\alpha_{sn}$  in order to gain insight into the physical transition from puffs to slugs. By definition a slug amounts to a region in parameter space where the leading edge moves faster than the trailing edge,  $v_l - v_t > 0$  (see [12] for this definition). This region is bounded by those combinations of parameters where both velocities match. We note that the leading edge velocity  $v_l(\alpha)$  is a function of  $\alpha$  only, and the trailing edge velocity  $v_t(h)$  depends solely on  $h$ . Consequently, the transition line  $\alpha_{PS}(h)$  can be found as root of the implicit function  $0 = F(\alpha, h) = v_l(\alpha) - v_t(h)$ , and in view of Fig. 4.1 it can be parameterized by the velocity  $v$ . We use a graphical algorithm based on Fig. 4.1 to solve  $v_l(\alpha) = v_t(h)$  for the implicitly-defined  $\alpha$ . Selecting a velocity  $v$  on the ordinate axis one can look up the respective intersections with the data  $v = v_l(\alpha)$  and  $v = v_t(h)$  and read off the corresponding values for  $\alpha$  and  $h$ . Hereby, we obtain a function  $\alpha(h)$ .

An example is given by the dotted gray line in Fig. 4.1 which starts off  $v = 0.18$ , and then identifies the corresponding control-parameter values of  $v_l(\alpha \simeq 2.61) = 0.18$  and  $v_t(h \simeq 2.16) = 0.18$  for the desired leading and trailing edge velocity, respectively. This provides the point  $\alpha_{PS}(h = 2.16) \simeq 2.61$  of the boundary  $\alpha_{PS}(h)$  separating regions where puffs and slugs are expected to arise. Varying  $v$  results in an implicit description of the boundary  $\alpha_{PS}(h)$ . The rule provides an accurate prediction for the transition threshold where slugs arise when increasing  $\alpha$  for a fixed value  $h \gtrsim 2.1$



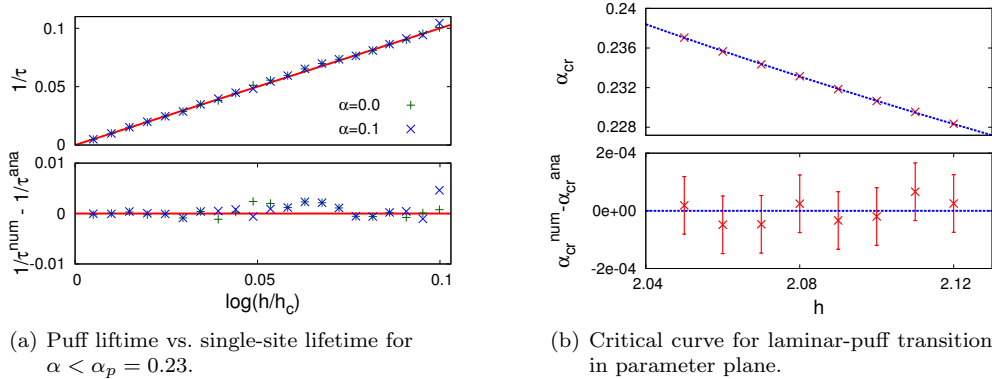


FIG. 4.3. (a) For  $\alpha < \alpha_P$  the lifetime follows exactly the prediction  $\tau = \tau_s \equiv [\ln(h/h_c)]^{-1}$  provided by the solid red line. The relative difference to the analytical prediction is shown in the lower panel. (b) Critical curve for the transition from a laminar state to a puff state. The implicitly-defined curve in Eq. (4.7) is shown as a blue dotted line. The results from numerical simulations (red crosses) are in perfect agreement with the analytical result. To show the accuracy of the prediction, the difference between the numerical results and analytical prediction Eq. (4.7) is shown in the lower panel. The errorbars reflect the discretization of the numerical data set.

(solid red line in Fig. 4.2).

**4.2. Puffs.** Close to the boundary for the transition from puffs to slugs one observes puffs with an exceedingly small probability to decay. Upon increasing  $h$  and decreasing  $\alpha$  the average lifetime of puffs decreases as indicated by the color code in Fig. 4.2. As long as  $\alpha > \alpha_P \simeq 0.23$  (solid black line in Fig. 4.2) the average lifetime  $\tau$  exceeds the one of the single-site dynamics by orders of magnitude; its parameter dependence will be discussed in Section 4.3. Below the threshold one exactly recovers the single-site lifetime as demonstrated in Fig. 4.3(a). The threshold coincides with the critical coupling strength where turbulence starts to propagate along the lattice, corresponding to the emerging of the first unstable coherent states, i. e., propagating wave-like solutions of the Navier-Stokes equation, in pipe flow. It amounts to the solution of the implicit equation

$$\alpha_P g(x_2^f) = \delta \quad \text{involving the fixed point} \quad x_2^f = \frac{h(2 + \delta)}{h + 1} \quad (4.7)$$

where  $f(x_2^f) = x_2^f$ . This equation expresses that the coupling reaches a level where repeated kicks, that appear when  $x^i$  takes the value of the right-most fixed point of  $f$ , can push site  $i + 1$  from the laminar into the chaotic state. It is not possible to trigger chaotic transients with the other fixed point  $x_1^f$  of  $f$ , since  $g(x_1^f) < 0$ . The prediction Eq. (4.7) is shown by the solid black line marking the lower border of the colored region in Fig. 4.2. This exact analytical result does not have any free fit parameters. It exactly agrees with the numerically determined threshold to an accuracy limited only by the numerical error of the order of  $10^{-4}$  (cf. Fig. 4.3(b)).

**4.3. Lifetime of Turbulent Puffs.** We now turn to the  $h$  dependence of the lifetime  $\tau$ . For  $\alpha > \alpha_P$  one observes a sharp increase of  $\tau$ ,

$$\ln \frac{\tau}{B} = C\tau_s, \quad \tau_s = \left[ \ln \frac{h}{h_c} \right]^{-1} \quad (4.8)$$

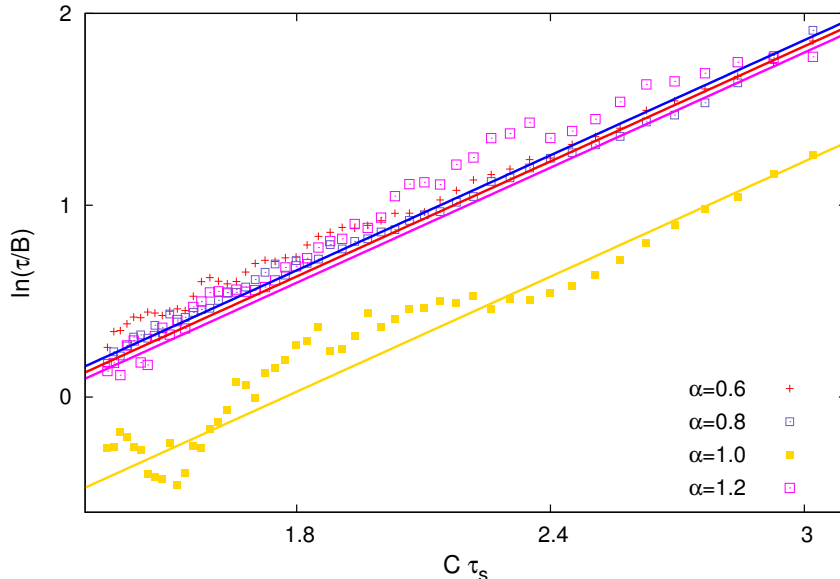


FIG. 4.4. Increase of the average lifetime  $\tau$  as function of  $\tau_s$ . Numerical data for different  $\alpha > \alpha_P$  (different points as indicated in the legend to the lower right) agree very well with the super-exponential scaling, Eq. (4.8).

when  $h$  approaches  $h_c = 2$  from above (see Fig. 4.4). The exponential increase identifies the finite-size traveling structures in this coupled map lattice as a new type of super-long transients [41]. As demonstrated in Fig. 4.4 the dependence Eq. (4.8) yields straight lines when  $\ln(\tau/B)$  is plotted as function of  $C\tau_s$  in agreement with the numerical data.

**5. Discussion.** We have introduced a coupled map lattice, Eq. (2.1), with a non-trivial unidirectional coupling, Eq. (2.2), between neighboring lattice sites. This dynamics has several interesting solutions, in particular in its transient behavior: (i) immediately decaying; (ii) structures with a fixed width that travel forward through the lattice (Fig. 3.1(a) and Fig. 3.1(b)); (iii) chaotic structures whose width grows linearly in time (Fig. 3.1(c)). We provided an analytical prediction of the lifetime of solutions of type (ii) which is in perfect agreement with numerical simulations (Fig. 4.3 and Fig. 4.4). Furthermore, we presented a mechanism for the transition between solutions of type (ii) and (iii), and we identified it as an unbinding transition. All results were obtained analytically as well as numerically. The analytical treatment revealed the fundamental mechanisms, i. e., the importance of the non-linear coupling, leading to different types of dynamics.

**5.1. Lifetimes of Puffs.** A simple statistical argument suggests that Eq. (4.8) might faithfully describe the lifetime of turbulent puffs. A dynamical systems representation of the transient turbulent dynamics should have  $\text{Re}^{9/4}$  active degrees of freedom which are sparsely coupled [19]. Moreover, the escape rate  $\kappa = \tau^{-1}$  amounts to the probability to enter the absorbing state where the motion proceeds directly to the laminar state [30]. Due to the nonlinear coupling between the modes this involves a constraint on a noticeably portion of the degrees of freedom. Applying this scaling to the slices of pipe flow that are described by single cells of our UCML provides a

scaling

$$\tau^{-1} \simeq B' \exp \left[ -C' \text{Re}^\beta \right] \quad \text{with } 1 \lesssim \beta \leq 9/4. \quad (5.1)$$

and appropriately adapted constants  $B'$  and  $C'$ .

Remarkably, this dependence is compatible with the findings of experimental pipe-flow data [20] where the authors supposed that their data are best fitted by

$$\tau^{-1} \simeq \exp \left[ -\exp(c_1 \text{Re} + c_2) \right] \quad \text{with } c_1 = 0.0057 \text{ and } c_2 = 8.7$$

while other adequate fits can also be obtained by other superexponential functions, in particular, by

$$\tau^{-1} \simeq \exp \left[ -(\text{Re}/c)^n \right] \quad \text{with } c = 1549 \text{ and } n = 9.95.$$

It is straightforward to check that the expression provided in Eq. (5.1) provides another very good fit of the experimental and numerical data in the relevant range,  $1650 < \text{Re} < 2050$ , of the Reynolds numbers considered in [20].

**5.2. Comparison to Other Approaches Addressing Pipe Flow with Dynamical Systems Tools.** We now compare the main features obtained for the UCML with those of previously published research addressing pipe flow with dynamical systems tools, in particular to the models of Barkley [7], Allhoff and Eckhardt [1] and Sipos and Goldenfeld [40]. Barkley's model [7] employs ideas from excitable media. It comprises a diffusively coupled map lattice in  $(1+1)$  dimensions and two variables with a non-linear coupling. The model is designed to mimic main features of pipe flow: turbulent puffs, puff splitting and turbulent slugs. A comparison to direct numerical simulations of pipe flow reveals qualitatively the same results after fitting of the main system parameter to experimental data. Unfortunately, the model has a rather big number of parameters. They are not studied and not compared to pipe flow, and severely hamper a theoretical analysis of the model. The main advantage of the presented UCML model over the model presented in [7] is the use of only a few parameters. This allowed us to provide an analytical treatment of its transitions and the parameter dependence of the lifetimes of transient structures. In principle we can also match the behaviour of pipe flow by relating the system parameters  $\alpha$  and  $h$  to  $\text{Re}$ . The limit  $h \rightarrow h_c = 2$  corresponds to a weaker decay to the laminar state, while an increase in  $\alpha$  indicates a stronger non-linear coupling. To comply with experiments, one hence should simultaneously increase  $\alpha$  and decrease  $h$  to  $h_c$ . Moreover,  $\delta$  and the slope of  $f$  and  $g$  at  $x = 0$  can be adjusted to account for the change of the stability of the laminar motion in pipe flow.

The models presented in [40] and [1] are directed percolation models and therefore stochastic by definition. Also there models were fitted to pipe flow data by appropriately adjusting their parameters. Since the Navier-Stokes equation is deterministic the comparison only applies to statistical quantities and does not give insight into the mechanisms from a dynamical systems perspective. The model of [1] is a  $(1+1)$ -dimensional model with two parameters and the one in [40] is  $(3+1)$ -dimensional and reduced to a  $(1+1)$ -dimensional model with one parameter. While [1] makes no prediction about the relation of the two system parameters to  $\text{Re}$ , [40] relates its control parameter  $p$  to  $\text{Re}$  in order to discuss the superexponential scaling of puff lifetime  $\tau(p)$ . Consequently, the superexponential scaling is not shown in [1], but the results are compared with mean field approximations. Puff splitting is only observed in [40] but not studied in detail.

**6. Conclusion and Outlook.** Coupled map lattices with a unidirectional nonlinear coupling capture salient features of turbulent pipe flow in terms of two parameters  $\alpha$  and  $h$ :

- (i) in reminiscence to the low Re regime of pipe flow all perturbations immediately decay to the laminar state when the coupling constant  $\alpha$  is small;
- (ii) for larger values of  $\alpha$  and sufficiently large  $h$  the model shows chaotic regions of a finite width that propagate down the pipe. These puff-like structures feature a lifetime statistics in accordance with super-long transients in dynamical systems;
- (iii) decreasing  $h$  leads to an unbinding transition of the leading and trailing edge of puffs, similar to the transition from puffs to slugs;
- (iv) there is an intermittent propagation of the leading edge of puffs and slugs (see the discussion in Section 4.1). These jumps have also been observed in real pipe flow. They comply with space-time plots of direct numerical simulations displayed in Refs. [12, 29, 4].

The UCML model uses less unknown parameters than the model presented in [7], and a better characterization is obtained by analytical results. All features were analyzed by explicit analytical calculations. In particular, we provided predictions for the parameter dependence of the transition lines and the lifetime of puffs. An interesting aspect of discussing the parameter dependences of our present UCML is that all its parameters have a well-defined physical interpretation for the pipe flow: the slopes of  $f$  and  $g$  at  $x = 0$  characterizes the linear stability of the laminar state,  $\delta$  describes the stability against finite-size perturbations,  $h$  relates to the leading Lyapunov exponent of turbulent states and  $\alpha$  is the strength of the nonlinear forward forcing in turbulent states. Hence, our analytical predictions connect the Re dependence of these features of the dynamics to the lifetime of transient structures and to the critical Re numbers that separate regimes where one observes stable laminar pipe flow, puffs, and slugs. Qualitatively, we expect that the limit  $h \rightarrow h_c = 2$  corresponds to a weaker decay to the laminar state, while an increase in  $\alpha$  indicates a stronger non-linear coupling. To comply with experiments, an increase in Re will therefore lead to a simultaneous increase of  $\alpha$  and decrease of  $h$  towards  $h_c$ .

Although the choice of a unidirectional, nonlinear coupling describes many features of pipe flow, it fails to faithfully cope with certain aspects of the dynamics. Arguably, the most prominent of these features is puff splitting, which is an important ingredient in the transition from puffs to slugs in real pipe flow. The onset of puff splitting is partly observed in Fig. 3.1, but much more analysis and appropriate modifications of the model will be necessary to obtain reliable results. After all, models with only nearest-neighbor coupling along the pipe can not be expected to capture the long-range coupling via the pressure that relaminarizes the leading puff unless it is separated by a sufficient distance [4].

Besides gaining insight into pipe flow, it is also of interest to study the dynamics of the unidirectionally coupled map lattice on its own. Beyond the realm of diffusive coupling not many coupled map lattice models have been studied analytically.

As an outlook, we mention that a probabilistic pendant to coupled map lattices is formalized in the theory of directed percolation [40] when one interprets the transition from puffs to slugs as threshold in directed percolation. The application of percolation to advectively-diffusively coupled map lattices has been studied in [10, 17, 16]. A comparison between our UCML and directed percolation invites further research. This future research can go into the direction of a systematic coarse graining to obtain the equivalent stochastic dynamics by means of symbolic dynamics. This coarse-graining

would then provide a rigorous connection to percolation theory.

**Acknowledgments.** The authors acknowledge very inspiring discussions with Reiner Kree, Arkadii Pikovsky, Antonio Politi, Lamberto Rondoni and Tamás Tél. They are grateful to Kerstin Avila and Björn Hof for sharing data prior to publication, and to Lamberto Rondoni and Tamás Tél for comments on a draft of the manuscript.

#### REFERENCES

- [1] KORINNA T ALLHOFF AND BRUNO ECKHARDT, *Directed percolation model for turbulence transition in shear flows*, Fluid Dynamics Research, 44 (2012), p. 031201.
- [2] E. G. ALTMANN, E. C. DA SILVA, AND I. L. CALDAS, *Recurrence time statistics for finite size intervals*, Chaos, 14 (2004), pp. 975–981.
- [3] EDUARDO G. ALTMANN, JEFFERSON S. E. PORTELA, AND TAMÁS TÉL, *Leaking chaotic systems*, Rev. Mod. Phys., 85 (2013), pp. 869–918.
- [4] K. AVILA, D. MOXEY, A. DE LOZAR, M. AVILA, D. BARKLEY, AND B. HOF, *The onset of turbulence in pipe flow*, Science, 333 (2011), pp. 192–196.
- [5] M. AVILA AND B. HOF, *Nature of laminar-turbulence intermittency in shear flows*, Phys. Rev. E, 87 (2013), p. 063012.
- [6] M. AVILA, A. P. WILLIS, AND B. HOF, *On the transient nature of localized pipe flow turbulence*, Journal of Fluid Mechanics, 646 (2010), pp. 127–136.
- [7] D. BARKLEY, *Simplifying the complexity of pipe flow*, Phys. Rev. E, 84 (2011), p. 016309.
- [8] L. A. BUNIMOVICH, R. LIVI, G. MARTINEZ-MEKLER, AND S. RUFFO, *Coupled trivial maps*, Chaos, 2 (1992), pp. 283–291.
- [9] L. A. BUNIMOVICH AND Y. G. SINAI, *Spacetime chaos in coupled map lattices*, Nonlinearity, 1 (1988), p. 491.
- [10] H. CHATÉ AND P. MANNEVILLE, *Spatio-temporal intermittency in coupled map lattices*, Physica D, 32 (1988), pp. 409–422.
- [11] G. COCHO AND G. MARTÍNEZ-MEKLER, *On a coupled map lattice formulation of the evolution of genetic sequences*, Physica D, 51 (1991), pp. 119 – 130.
- [12] Y. DUGUET, A. P. WILLIS, AND R. R. KERSWELL, *Slug genesis in cylindrical pipe flow*, J. Fluid Mech., 663 (2010), pp. 180–208.
- [13] H. FAISST AND B. ECKHARDT, *Sensitive dependence on initial conditions in transition to turbulence in pipe flow*, J. Fluid Mech., 504 (2004), pp. 343–352.
- [14] H. GANG AND Q. ZHILIN, *Controlling spatiotemporal chaos in coupled map lattice systems*, Phys. Rev. Lett., 72 (1994), pp. 68–71.
- [15] F. GINELLI, R. LIVI, AND A. POLITI, *Emergence of chaotic behaviour in linearly stable systems*, Journal of Physics A, 35 (2002), p. 499.
- [16] F. GINELLI, R. LIVI, A. POLITI, AND A. TORCINI, *Relationship between directed percolation and the synchronization transition in spatially extended systems*, Phys. Rev. E, 67 (2003), p. 046217.
- [17] P. GRASSBERGER AND T. SCHREIBER, *Phase transitions in coupled map lattices*, Physica D, 50 (1991), pp. 177–188.
- [18] C. GREBOGI, E. OTT, AND J. A. YORKE, *Chaotic attractors in crisis*, Phys. Rev. Lett., 48 (1982), pp. 1507–1510.
- [19] S. GROSSMANN, *The onset of shear flow turbulence*, Rev. Mod. Phys., 72 (2000), pp. 603–618.
- [20] B. HOF, A. DE LOZAR, D. J. KUIK, AND J. WESTERWEEL, *Repeller or attractor? Selecting the dynamical model for the onset of turbulence in pipe flow*, Phys. Rev. Lett., 101 (2008), p. 214501.
- [21] B. HOF, A. JUEL, AND T. MULLIN, *Scaling of the turbulence transition threshold in a pipe*, Phys. Rev. Lett., 91 (2003), p. 244502.
- [22] B. HOF, J. WESTERWEEL, T. M. SCHNEIDER, AND B. ECKHARDT, *Finite lifetime of turbulence in shear flows*, Nature, 443 (2006).
- [23] K. KANEKO, *Turbulence in coupled map lattices*, Physica D, 18 (1986), p. 475.
- [24] ———, *Spatiotemporal chaos in one- and two-dimensional coupled map lattices*, Physica D, 37 (1989), pp. 60 – 82.
- [25] ———, *Supertransients, spatiotemporal intermittency and stability of fully developed spatiotemporal chaos*, Phys. Lett. A, 149 (1990), pp. 105–112.
- [26] J. D. C. LITTLE, *A proof for the queuing formula -  $L=\lambda \cdot W$* , Oper. Res., 9 (1961), pp. 383–387.
- [27] F. MELLIBOVSKY, A. MESEGUER, T. M. SCHNEIDER, AND B. ECKHARDT, *Transition in localized pipe flow turbulence*, Phys. Rev. Lett., 103 (2009).

- [28] A. MESEGUER AND L. N. TREFETHEN, *Linearized pipe flow to Reynolds number  $10^7$* , J. Comp. Phys., 186 (2003), pp. 178 – 197.
- [29] D. MOXEY AND D. BARKLEY, *Distinct large-scale turbulent-laminar states in transitional pipe flow*, PNAS, 107 (2010), pp. 8091–8096.
- [30] E. OTT, *Chaos in Dynamical Systems*, Cambridge University Press, 2002.
- [31] N. PAREKH, S. PARTHASARATHY, AND S. SINHA, *Global and local control of spatiotemporal chaos in coupled map lattices*, Phys. Rev. Lett., 81 (1998), pp. 1401–1404.
- [32] P. PARMANANDA, M. HILDEBRAND, AND M. EISWIRTH, *Controlling turbulence in coupled map lattice systems using feedback techniques*, Phys. Rev. E, 56 (1997), pp. 239–244.
- [33] J. PEIXINHO AND T. MULLIN, *Decay of turbulence in pipe flow*, Phys. Rev. Lett., 96 (2006).
- [34] Y. POMEAU, *Front motion, metastability and subcritical bifurcations in hydrodynamics*, Physica D, 23 (1986), pp. 3 – 11.
- [35] Y. POMEAU, *Localised chaos in extended geometries*, Helv. Phys. Acta (Switzerland), 62 (1989), pp. 542–543.
- [36] Y. POMEAU AND P. MANNEVILLE, *Intermittent transition to turbulence in dissipative dynamical systems*, Commun. Math. Phys., 74 (1980), p. 189.
- [37] O. REYNOLDS, *An experimental investigation of the circumstances which determine whether the motion of water shall be direct or sinuous, and of the law of resistance in parallel channels*, Phil. Trans. R. Soc. Lond., 174 (1883), p. 935.
- [38] O. RUDZICK AND A. PIKOVSKY, *Unidirectionally coupled map lattice as a model for open flow systems*, Phys. Rev. E, 54 (1996), pp. 5107–5115.
- [39] O. RUDZICK, A. PIKOVSKY, C. SCHEFFCZYK, AND J. KURTHS, *Dynamics of chaos-order interface in coupled map lattices*, Physica D, 103 (1997), pp. 330 – 347.
- [40] M. SIPOS AND N. GOLDENFELD, *Directed percolation describes lifetime and growth of turbulent puffs and slugs*, Phys. Rev. E, 84 (2011), p. 035304.
- [41] T. TÉL AND Y.-C. LAI, *Chaotic transients in spatially extended systems*, Physics Reports, 460 (2008), pp. 245 – 275.
- [42] F. H. WILLEBOORDSE, *Supertransients and suppressed chaos in the diffusively coupled logistic lattice*, Chaos, 4 (1994), pp. 89–98.
- [43] I. WYGNANSKI AND F. CHAMPAGNE, *On transition in a pipe. I. the origin of puffs and slugs and the flow in a turbulent slug*, J. Fluid Mech., 59 (1973), pp. 281–235.
- [44] S. YUKAWA AND M. KIKUCHI, *Coupled-map modeling of one-dimensional traffic flow*, Journal of the Physical Society of Japan, 64 (1995), pp. 35–38.